N00014-18-1-2514: 3D PRINTING OF MAGNETIC CORES FOR ELECTRICAL MOTORS

FINAL PERFORMANCE REPORT

August 2022

Shanelle N. Foster, Assistant Professor
Department of Electrical and Computer Engineering
Michigan State University
East Lansing, MI

EXECUTIVE SUMMARY

Expanded use of electrical machines on naval ships increase energy efficiency; however, deploying ships with spare motors and generators may not be feasible and getting parts to ships at sea is also a challenge. 3D printing can potentially eliminate the logistical nightmares of maintenance and replacing electrical machines on deployed naval ships. Additionally, the availability of practical additive manufacturing techniques that provide acceptable electrical, magnetic and mechanical properties for the magnetic core will accelerate the development of power dense and efficient 3D printed electric motors and generators.

An integrated set of experiments, summarized in Fig. 1, were used to expand the knowledge base that pertains to functional and structural characteristics of deposited iron alloys for design of magnetic cores in electrical machines, transformers and other magnetic assemblies.

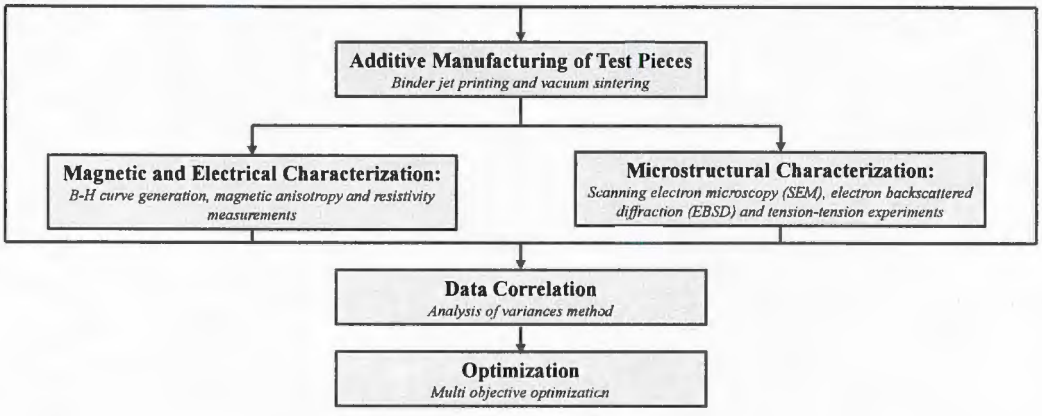

Figure 1: Iterative process utilized to develop binder jet printed with acceptable magnetic properties.

This report briefly summarizes development of magnetic cores using binder jet printing technology via the investigation of the material magnetic properties. Eighty (80) samples were prepared with different material compositions and process parameters. Soft magnetic composite material (SMC) was used as the baseline comparison for this work primarily because SMC has been used for construction of unconventional motor topologies. The addition of boron as a sintering aid is shown to improve the performance of binder jet printed magnetic cores. Boron results in a eutectic reaction of Fe_2B and Fe at 1174°C, which shows as grain-boundary lamellae phase. It is shown that the magnetic relative permeability of the optimized binder jet printed magnetic cores is nearly 6 times that of SMC [1]. The optimized binder jet printed magnetic core also has lower hysteresis loss per cycle than commercially available SMC [1]. The magnetic saturation flux density of the optimized binder jet printed magnetic core is 1.5T, similar to the maximum for commercially available SMC [1].

A permanent magnet motor was designed and assembled using a binder jet printed magnetic core with cooling channels in each tooth. This particular design was enabled by the flexibility of 3D printing technologies. The motor was mounted and experimentally evaluated.

ACKNOWLEDGMENTS

Thank you to following people for their support of this project:

- Dr. Jenn Wolk. ONR 33 Program Officer
- Prof. Kalyanmoy Deb, MSU Department of Electrical and Computer Engineering
- Dr. Per Askeland, MSU Composite Materials and Structures Center

Additionally, thank you to the CNR Concept Challenge for spearheading this opportunity.

TABLE OF CONTENTS

LIST OF TABLES

LIST OF FIGURES

Chapter 1

Introduction

The magnetic stator and rotor cores play a key role in the energy conversion of electric motors as it is used for creation of magnetic flux in the air gap for electromagnetic torque production. Accurate knowledge of the magnetic and electrical properties of the core is critical to designing high performance, low cost electric motors that can revolutionize electric motor manufacturing. It is desirable to expand the use of 3D printed ferromagnetic alloys beyond structural applications to include those requiring functional properties, as is the case for electric motors. Some of the desired magnetic properties for the magnetic core of electric motors include high permeability at low field strength, high saturation, low hysteresis loss and low eddy current loss.

Additive manufacturing technologies have been used to build motor cores; however, the magnetic properties of 3D printed cores have not been adequately explored in the literature or engineering practice. Selective laser melting has been investigated for depositing ferromagnetic alloys. With this additive manufacturing technology, the laser power and laser spot size are adjusted to fully melt the powder to develop a highly dense part without post-processing; however, instability in the molten pool can lead to delamination and cracks. Binder jet printing does not use a laser to melt the powder but instead a sintering process is used to burn off the binder and solidify the part. Although post-processing is utilized with this additive manufacturing technology, binder jet printing can be considered a cost-effective technology.

It is well known that the microstructural parameters, including grain size, inclusions, and internal stresses, have a strong influence on magnetic properties. These relationships in 3D printed ferromagnetic alloys are not well understood; however, electrical steel laminations and soft magnetic composites(SMC) offer some insight. The effects of grain size on the magnetic properties of laminations has been evaluated. It is known that the magnetic induction and permeability are influenced by the crystallographic texture. Bloch wall displacements, called Barkhausen jumps, result in hysteresis generally due to the defects in the crystals. Both impurities in the iron particles and at the grain boundaries and stress increase pinning of the domain walls and increase hysteresis loss. Plastic deformation also affects hysteresis loss. Low frequencies, large particle sizes, higher purity iron and annealing can reduce hysteresis loss. Higher purity iron also has high magnetic saturation flux density. Silicon and insulated iron powders have been used to increase the resistivity of iron powder. The insulated iron powders, used in soft magnetic composites (SMCs), have a non-magnetic space between each particle, which negatively impacts magnetic permeability, magnetic flux density and strength; however, the isotropic three-dimensional flux path, as enabled by SMC, has been shown to benefit unconventional motor topologies, such as those involved in the

axial flux, transverse flux, and claw pole motors. Increasing the particle size increases the permeability and the maximum flux density, but reduces the resistivity and the strength. The addition of a binder to the powder, high compaction pressure and heat treatment all increase strength of SMCs; however, the binder reduces the magnetic permeability and the maximum flux density.

Chapter 2

Major Goals and Objectives

The overall objective of the project was to promote development of a 3D printed magnetic core with desirable magnetic properties for electric motors. We accomplished the overall objective of the proposed project through the following tasks:

Task 1: Magnetic Core Characterization The tasks were aimed to define the relationship across material composition, process parameters and functional properties of 3D printed alloys.

- Further characterization of the off-the-shelf silicon iron powder using energy dispersive spectroscopy (EDS) qualitatively estimate the powder composition.
- Subsequent test samples were prepared with varying process parameters and material composition, including the binder composition, composition of the iron alloy, mean particle sizes, and sintering temperature.
- Electrical and magnetic characterization was carried out for each variation
- Quantified the significance of each process parameter and material composition using its sensitivity.

Task 2: Magnetic Core Model Development The tasks were aimed to define the relationship across microstructure, material composition, process parameters, and functional properties of 3D printed alloys.

- Developed a regression model using the acquired characterization data, process parameters and material composition.
- Test samples were prepared with varying process parameters and material composition. The initial variation was guided by the results of previous and subsequent tasks.
- Microstructural, electrical and magnetic characterization was carried out for each variation.
- The relationships and interrelationships between process parameters, microstructure and magnetic properties was quantified using a multivariate ANOVA method.

Task 3: Magnetic Core Optimization and Validation The tasks were aimed to develop a 3D printed magnetic core with optimized electrical and magnetic properties.

- Applied the Non-dominated Sorting Genetic Algorithm (NSGA) to obtain trade-off solutions.

- The obtained trade-off solutions were mined for deciphering common features associated with them. These features remained as design principles and helped provide key insights to processing iron alloys with optimal magnetic properties using binder jet printing processes.
- Prepared test samples using the process parameters and material composition of a few Pareto optimal solutions.
- Evaluated the mechanical, electrical and magnetic properties of the Pareto optimal solutions.
- Designed and assembled a permanent magnet motor with 3D printed magnetic core.
- Evaluated the performance of an electric motor with finite elements having the Pareto optimal solutions as the magnetic core.

Chapter 3

Accomplishments Under Goals

The following milestones were met:

Milestone 1.1: Identified boron had the greatest significance on the magnetic properties. As expected, silicon impacted loss density. Magnetic anisotropy was not impacted by material composition nor temperature. Details of the process parameters and its impact on magnetic properties will be included in the PhD thesis under preparation by Hawke Suen, a project participant.

Milestone 2.1: Identified grain size and the presence of an Fe_2B grain-boundary lamellae phase had the greatest significance on the magnetic properties. The addition of boron

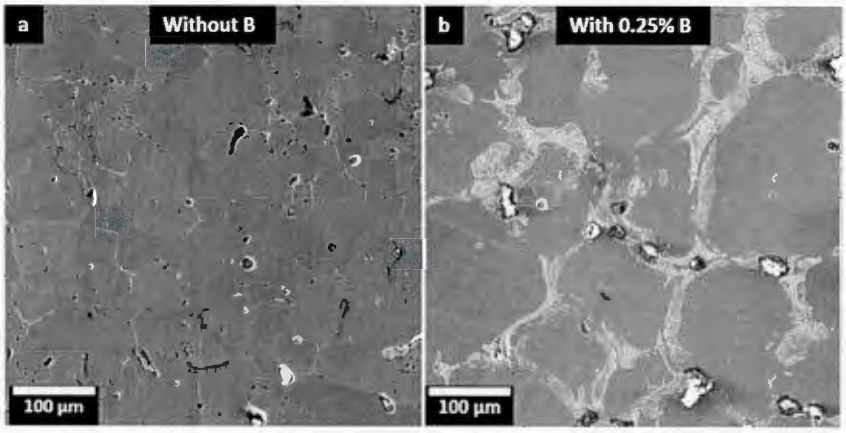

Figure 3.1: Comparison of grain-boundary for samples with and without boron. Both samples are $Fe_{95}Si_5$ sintered at 1200°C. The $F2_2B$ grain-boundary lamellae phase is present in the sample with boron.

increased hardness as shown in Fig. 3.2. Silicon content had the greatest impact on relative density of the final part. These findings are discussed in [2], which is currently under review.

Milestone 2.2: Identified the interrelationship between silicon and boron had the greatest significance on the magnetic properties. Though the temperature does not show an impact on the magnetic properties, the interaction of boron and temperature impacts relative density of the final part. Both boron and silicon are sintering aids thereby requiring temperature modifications to reduce shape distortion of the final part.

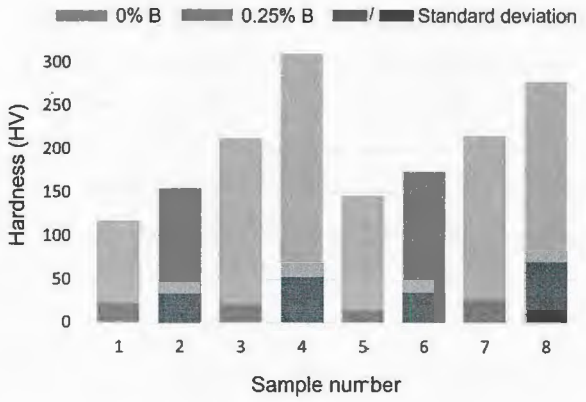

Figure 3.2: Comparison of Vickers Hardness for samples with and without boron. Samples 1 and 2 are $Fe_{97}Si_3$ sintered at 1200°C. Samples 3 and 4 are $Fe_{95}Si_5$ sintered at 1200°C. Samples 5 and 6 are $Fe_{97}Si_3$ sintered at 1250°C. Samples 7 and 8 are $Fe_{95}Si_5$ sintered at 1250°C.

Milestone 2.3: Demonstrated through magnetic characterization of additional samples that the regression models for magnetic relative permeability, coercive force, loss density and relative density held.

Milestone 3.1: Identified the following principles for binder jet printing optimal magnetic cores: (1) 0.25% boron, independent of the silicon content, improves overall performance and (2) sintering temperatures less than or equal to 1200°C improves overall magnetic performance. Boron increased the grain size and rounded corners of the grains, as shown in Fig. 3.3. The increased grain size allows multiple magnetic

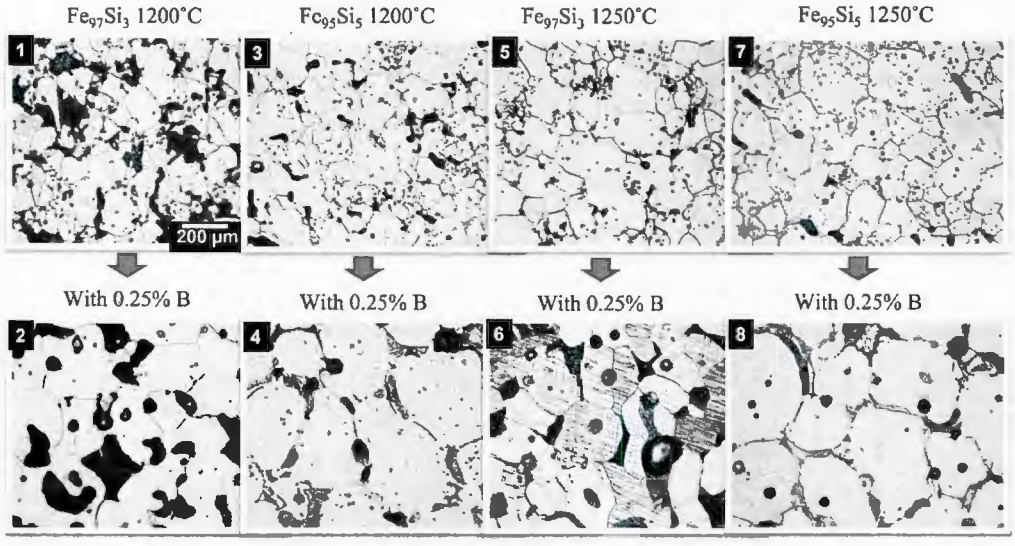

Figure 3.3: Optical photomicrographs of etched samples at same magnification. The addition of boron increases grain size.

domains in a single grain, resulting in increased magnetic permeability and induction. The rounded corners helped reduce pinning of the magnetic domain wall, thereby reducing hysteresis loss, Fig. 3.4. These findings are discussed in [2], which is currently under review.

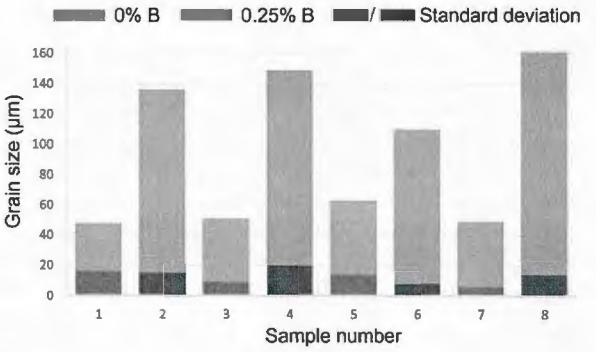

Figure 3.4: Comparison of hysteresis loss for samples with and without boron. Samples 1 and 2 are $Fe_{97}Si_3$ sintered at 1200°C. Samples 3 and 4 are $Fe_{95}Si_5$ sintered at 1200°C. Samples 5 and 6 are $Fe_{97}Si_3$ sintered at 1250°C. Samples 7 and 8 are $Fe_{95}Si_5$ sintered at 1250°C.

Milestone 3.2: Demonstrated through magnetic, electrical and microstructural characterization the improved performance of Pareto optimal material compositions and sintering temperature, independent of the powder source. Powders were sourced from GoodFellow, American Elements, Carpenter Additive and Oerlikron. Further analysis of the boron particle size, without variations in material composition or sintering temperature, impacts loss density. Reducing the boron particle size one tenth resulted in improved performance, including lower dynamic loss, as shown in Figs. 3.5 and 3.6 These findings are described in [3]. The impact of the boron particle

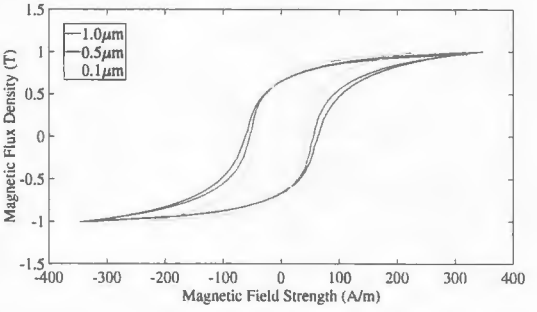

Figure 3.5: Experimentally extracted BH loops of BJP samples with different boron particle size at 1 T.

size on performance of an electric motor is described in [4].

Milestone 3.3: An electric motor was designed. Its stator core was fabricated using one of the Pareto optimal material compositions and sintering temperature. The electric

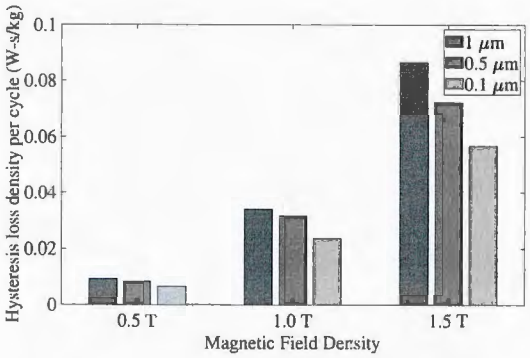

Figure 3.6: Illustration of impact of boron additive particle size on hysteresis loss density per cycle of BJP samples.

motor was assembled and experimentally evaluated. The 3D printed magnetic core was fabricated with cooling channels to capitalize on the benefit of additive manufacturing. A comparison of thermal performance of the electric motor fabricated with the 3D printed magnetic core will be compared to an SMC core in a dissertation (currently under preparation) by Matt Meier, a participant on this project.

3.1 Performance Comparison of Developed 3D Printed Cores

Samples of both commercially available M19 electrical steel and Siron 280b (an SMC) were used as comparison. The magnetic properties of the samples were experimentally extracted and compared with the manufacturers data sheet prior to comparison with binder jet printed magnetic cores, Fig. 3.7. The maximum magnetic relative permeability of the

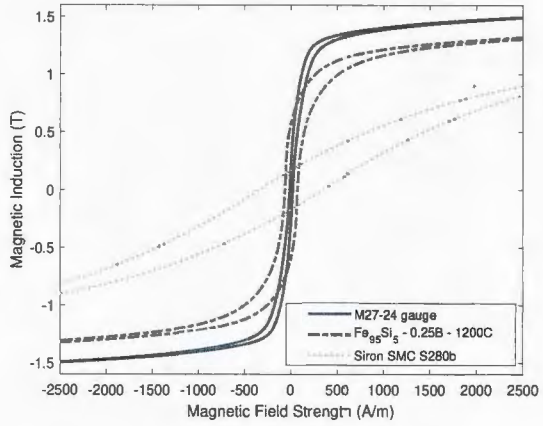

Figure 3.7: Experimental quasi-static hysteresis loops comparing a laminated iron silicon (M19 electrical steel), a binder jet printed sample, and Siron 280b (SMC) sample.

binder jet printed magnetic cores exceed that of both samples. However, it is worth noting

there are other electrical steels commercially available that exceed the permeability of the M19 sample and the binder jet printed samples. There are also commercially available SMC that exceed the permeability of Siron 280b; however, based on information from their data sheet they do not exceed the permeability of the binder jet printed samples. The magnetic saturation flux density of the binder jet printed samples is lower than M19 electrical steel as well as other commercially available electrical steels. However, the flux density of the developed 3D printed samples outperforms the SMC sample and other commercially available SMCs [1]. The M19 sample has superior specific loss density. At low frequency, the binder jet printed samples outperform the SMC sample. As the frequency increases, SMC has significantly lower loss than the developed 3D printed samples. The value of the magnetic coercive force is an indicator of the hysteresis loss. The magnetic coercive force of the binder jet printed samples is within range of commercially available electrical steels [1].

The level of magnetic anisotropy can be quantified by the differences in the magnetic field strength required to reach the same level of magnetic induction under different excitation directions.

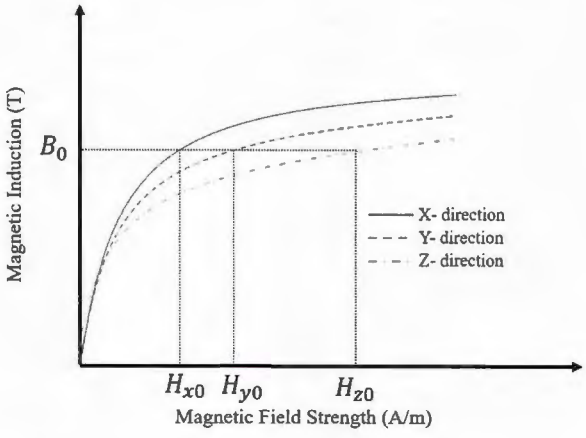

Figure 3.8: Illustration of the magnetization curves of soft magnetic materials experiencing magnetic anisotropy under excitation in X-, Y-, and Z- directions.

For a soft magnetic sample experiencing magnetic anisotropy, as illustrated in Fig. 3.8, the magnetic induction B_0 is reached at different magnetic field strength for different excitation directions. These differences can be used to quantify the level of anisotropy as described in (3.1) and (3.2). Here, Δ_y is the difference in percentage between the H_{y0}, compared H_{x0}, when calculated at the same magnetic induction B_0. Similarly, Δ_z is the difference in percentage between the H_{z0}, compared H_{x0}, when calculated at the same magnetic induction B_0. The

$$\Delta_y = \frac{H_{y0} - H_{x0}}{H_{x0}} \tag{3.1}$$

$$\Delta_z = \frac{H_{z0} - H_{x0}}{H_{x0}} \tag{3.2}$$

The levels of magnetic anisotropy of Siron 280b and the binder jet printed samples were found similar, as shown in Fig. 3.9 and Table 3.1. Magnetic anisotropy of M19 was not

evaluated because stacks of thin sheets of electrical steel will yield high levels of anisotropy in the stacking direction due to the air gaps and insulation on each sheet.

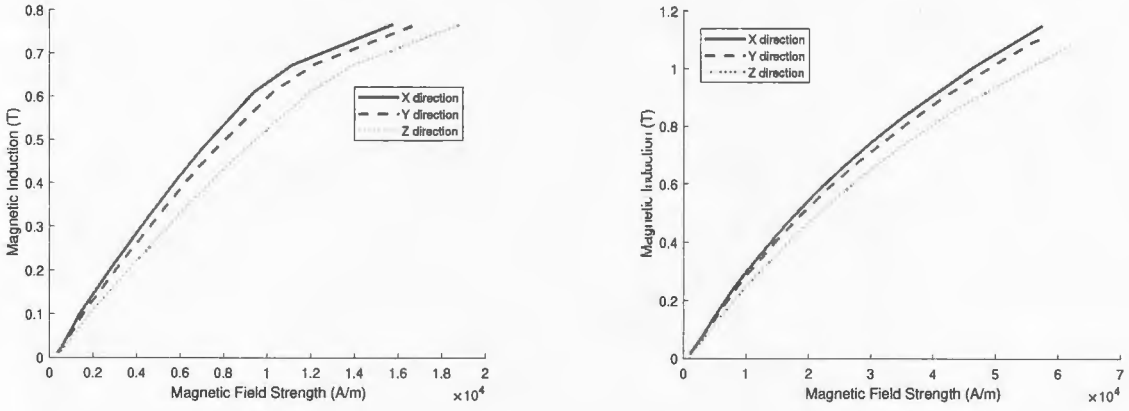

(a) SMC (b) BJP

Figure 3.9: Magnetization curves of SMC and BJP cubes under x-, y-, and z-directions. The excitation frequency is 50Hz. The magnetic field strength is calculated under open magnetic circuit characterization using the simplified magnetic anisotropy characterization test bed described in Appendix B.

Table 3.1: Comparison of magnetic anisotropy between SMC and 3D printed iron silicon. Magnetic anisotropy quantifiers are calculated at 0.25 T, 0.5 T, 0.75 T, and 1.0 T.

Magnetic	SMC cube		3D printed cube	
induction B_0	Δ_y	Δ_z	Δ_y	Δ_z
0.25 T	9.3%	29.8%	4.6%	22%
0.5 T	9%	28%	5.4%	20%
0.75 T	7%	20.5%	6.3%	19.4%
1.0 T	N/A	N/A	6%	20%

The magnetic performance of the developed 3D printed samples is discussed [3–11]. The results of optimization identified $Fe_{95}Si_5$ with 0.25 B sintered at 1200°C as a Pareto optimal solution. The ranges for magnetic relative permeability, coercivity and magnetic saturation flux density of the binder jet printed samples fabricated as shown in Table 3.2.

Table 3.2: Ranges for experimental magnetic properties for the 80 printed samples.

Magnetic Property	Range
Relative permeability	$1,828 - 7,861$
Coercivity	$41 - 104$ A/m
Saturation flux density	$B_{sat} = 1.3 - 1.63T$

3.2 Assembly and Performance of Electric Motor

$Fe_{95}Si_5$ with 0.25%B was used to fabricate the stator core of an axial flux permanent magnet (AFPM) motor . Capitalizing on the flexibility of the binder jet printing technology, cooling channels were embedded in the design of the stator core. Due to the limited bed size and the need to remove powder from the cooling channels, the stator core was printed in 14 separate parts, as shown in Fig. 3.10. The parts were assembled and sintered at 1200°C.

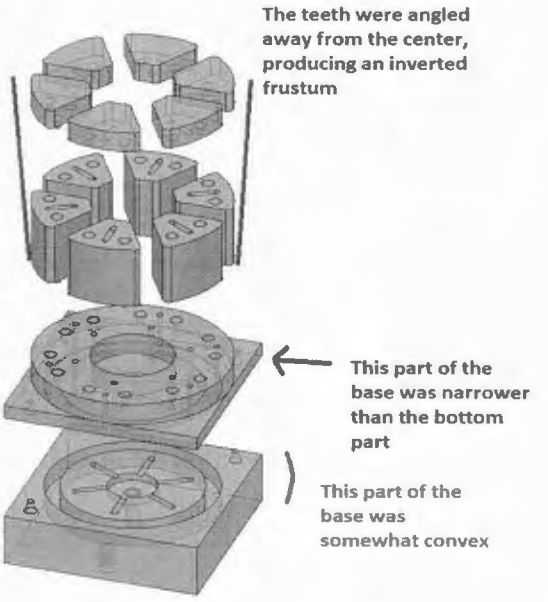

Figure 3.10: Illustration of the 3D printed stator magnetic core assembly with cooling channels.

The final 3D printed stator magnetic core is shown in Fig. 3.11a.

The stator was assembled using Nomex paper, copper windings, and a baseplate fixture including the connections to inlet and outlet of the chiller, inverter and thermocouples Fig. 3.11b. The permanent magnet rotor, shown in Fig. 3.12a was also assembled. The completed axial flux permanent magnet motor was mounted on a dynamometer for

(a) Stator magnetic core

(b) Stator assembly

Figure 3.11: Pictures of 3D printed stator magnetic core with cooling channels after sintering and full stator core assembly.

(a) PM rotor

(b) AFPM motor with 3D printed core

Figure 3.12: Pictures of the axial flux permanent magnet motor with 3D printed stator core connected to the dynamometer.

experimental evaluation as shown in Fig. 3.12b. The measured induced voltage closely approximates the finite element simulation results, as shown in Fig. 3.13. Results of the thermal performance comparison of the AFPM motor with the 3D printed core to the SMC core across a wide speed range will be included in the PhD thesis under preparation by Matt Meier, a project participant.

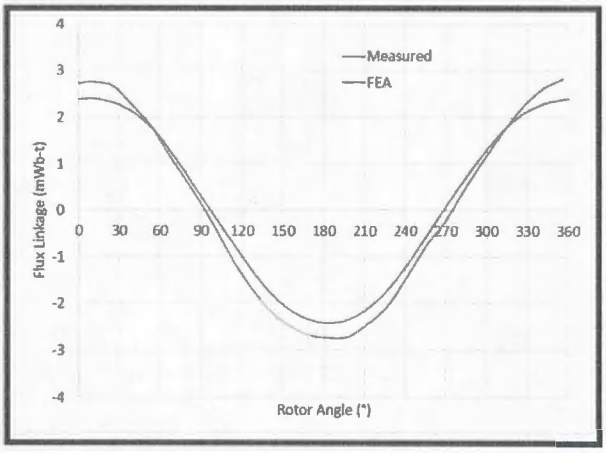

Figure 3.13: Comparison of experimental and finite element induced voltage for axial flux permanen magnet motor with 3D printed stator core.

Chapter 4

Results Dissemination

4.1 Journal Articles

[1] G. Kumari, T. Q. Pham, H. Suen, T. Rahman, P. Kwon, S. N. Foster, and C. J. Boehlert, "Improving the soft magnetic properties of binder jet printed iron-silicon alloy through boron addition," Materials Chemistry and Physics, **Under Review**.

Abstract: Fe-Si alloys are an essential class of soft magnetic materials due to their high magnetic permeability and low hysteresis loss. Increasing the Si content above 3wt.% enhances the magnetic properties, but it makes the material brittle and difficult for machining. This work investigated the effects of Si content, which ranged from 3 to 5wt.% and B content, which ranged from 0 to 0.25wt.%. Fe-Si-B based soft magnets were printed via binder jet printing using B as a sintering additive, and the sintering temperature was varied between 1200 to 1250°C. The relationship between microstructure and magnetic properties was investigated based on the characterization of magnetic permeability, intrinsic coercivity, grain size, grain boundary phase, and density. The results shows that the composition of Fe 95 Si 5 with 0.25% B sintered at 1200°C exhibited the highest magnetic permeability (3475 A/m) and the lowest intrinsic coercivity (69.6 A/m).

[2] T. Q. Pham, H. Suen, P. Kwon, G. Kumari, C. J. Boehlert and S. N. Foster, "Reduction in Hysteresis Loss of Binder Jet Printed Iron Silicon With Boron," in IEEE Transactions on Industry Applications, vol. 57, no. 5, pp. 4864-4873, Sept.-Oct. 2021, doi: 10.1109/TIA.2021.3099463.

Abstract: In this article, we use a factorial design of experiments to develop a three-way relationship between the 3-D printing parameters, the microstructural characteristics, and the hysteresis loss of binder jet printed iron silicon. Subsequent analysis of variance is used to validate the hypotheses between the printing process input factors and the output factors. The input factors in this work include the sintering temperature, the addition of boron, and the silicon content in the starting powder. The magnetic output factors of the printed iron silicon include the intrinsic coercivity and the hysteresis loss per cycle, which are extracted via the use of quasi-static magnetic characterization. Additionally, ac magnetic characterization is used to extract the total iron loss of the binder jet printed silicon. The microstructural output factors are extracted via the use of optical microscope. The established relationship can be used to reduce hysteresis loss in binder jet printed iron silicon.

[3] T. Pham, P. Kwon, and S. Foster, "Additive manufacturing and topology optimization of magnetic materials for electrical machines - a review," Energies, vol. 14, no. 2, 2021. [Online]. Available: https://www.mdpi.com/1996-1073/14/2/283

Abstract: Additive manufacturing has many advantages over traditional manufacturing methods and has been increasingly used in medical, aerospace, and automotive applications. The flexibility of additive manufacturing technologies to fabricate complex geometries from copper, polymer, and ferrous materials presents unique opportunities for new design concepts and improved machine power density without significantly increasing production and prototyping cost. Topology optimization investigates the optimal distribution of single or multiple materials within a defined design space, and can lead to unique geometries not realizable with conventional optimization techniques. As an enabling technology, additive manufacturing provides an opportunity for machine designers to overcome the current manufacturing limitation that inhibit adoption of topology optimization. Successful integration of additive manufacturing and topology optimization for fabricating magnetic components for electrical machines can enable new tools for electrical machine designers. This article presents a comprehensive review of the latest achievements in the application of additive manufacturing, topology optimization, and their integration for electrical machines and their magnetic components.

4.2 Conference Paper

[1] B. Khoshoo, K. J. Islam, H. Suen, P. Kwon, J. Peña Lozano, and S. N. Foster, "Eddy current loss reduction in binder jet printed iron silicon cores," in 2022 International Conference on Electrical Machines (ICEM), **Accepted**.

Abstract: Additive manufacturing of soft magnetic iron cores can help realize electric machines with increased power density. However, high eddy current loss in the 3D printed bulk iron core is a big challenge before AM can be used for commercial production of electric machines. It is possible to realize lower eddy current loss by improving the chemical composition of the material at microstructure level. This article discusses a method to reduce the specific loss density of 3D printed iron cores using binder jet printing. It is shown that reducing the size of boron particle, used as a sintering aid, results in lower core loss without significant change in magnetization of the sample. Extracted material properties of presented samples are further validated by finite element simulations using a permanent magnet machine. Performance comparison in the entire torque/speed envelop shows eddy current loss reduction and efficiency improvement with increase in speed.

[2] K. J. Islam, T. Q. Pham, H. Suen, G. Kumari, T. Rahman, C. J. Boehlert, P. Kwon, and S. N. Foster, "Eddy current loss reduction in binder jet printed iron silicon," in 2022 IEEE Energy Conversion Congress and Exposition (ECCE), **Accepted**.

Abstract: One of the key features of any electric machine is high efficiency, which in turn means keeping losses to a minimum.Recent advances in the field of additive manufacturing show that the addition of boron to binder jet printed iron silicon improves magnetic properties. However, there has been little success in reducing the eddy current losses at higher frequencies. In this work, the effect of boron particle size on total loss in binder jet printed iron silicon steel was evaluated. Both quasi-static and ac magnetic characterization were used to analyze the magnetic properties. Bulk resistivity is measured using four-probe method. Finally, the microstructure was analyzed using scanning electron microscopy to study the grain boundary as well as quantify the grain size and porosity.

[3] T. Q. Pham and S. N. Foster, "Multi-permeability optimization approach for the iron core of a synchronous reluctance machine - an application of additive manufacturing," 2021 IEEE Energy Conversion Congress and Exposition (ECCE), 2021, pp. 3852-3859, doi: 10.1109/ECCE47101.2021.9595987.

Abstract: Electrical machine design optimization has typically been used to identify geometric variables that best help meet certain performance objectives. Topology optimization techniques allow distribution of materials to identify unique electrical machine designs. Here, a technique is presented to optimize distribution of material properties within the iron core, specifically the magnetic permeability, to meet a certain performance objective instead of varying geometric variables. The tool uses the reluctance network in lieu of finite element analysis to estimate the airgap flux density with a lower computational effort, without sacrificing accuracy.

[4] T. Q. Pham and S. N. Foster, "Additive Manufacturing of Non-homogeneous Magnetic Cores for Electrical Machines Opportunities and Challenges," 2020 International Conference on Electrical Machines (ICEM), 2020, pp. 1623-1629, doi: 10.1109/ICEM49940.2020.9270978.

Abstract: Maturation of additive manufacturing technologies present opportunities for development of non-conventional soft magnetic materials. In this paper, it is demonstrated that manipulation of the magnetic properties of magnetic cores can be used to shape the magnetic flux density in the air-gap. A simple finite element program is used to evaluate the stator pole of an electrical machine with non-homogeneous magnetic properties. This paper shows a potential advantage of using additive manufacturing for development of magnetic cores with non-homogeneous magnetic property in electrical machines.

[5] T. Q. Pham, H. Suen, P. Kwon and S. N. Foster, "Reduction in Hysteresis Loss of Binder Jet Printed Iron Silicon," 2020 International Conference on Electrical Machines (ICEM), 2020, pp. 1669-1675, doi: 10.1109/ICEM49940.2020.9270774.

Abstract: In this paper, the hysteresis loss characteristics of 3D printed iron silicon samples are compared with soft magnetic composite material. Design of experiments

is used to evaluate the effect of printing parameters on hysteresis loss. Printing parameters considered in this paper include the sintering temperature, the addition of boron compound, and the silicon content in the starting powder. The addition of boron in the 3D printing process of iron silicon samples is shown to reduce the intrinsic coercivity and hysteresis loss.

[6] T. Q. Pham, H. Suen, P. Kwon and S. N. Foster, "Characterization of Magnetic Anisotropy for Binder Jet Printed Fe93.25Si6.75," 2019 IEEE Energy Conversion Congress and Exposition (ECCE), 2019, pp. 745-752, doi: 10.1109/ECCE.2019.8913105.

Abstract: Isotropic magnetic properties are important for electrical machine topologies that require 3D flux paths. Soft magnetic composites, which have been used to manufacture magnetic cores for these designs, have limitations. Additive manufacturing technologies provide flexibility to fabricate ferromagnetic structures that can overcome challenges inherent in manufacturing soft magnetic composites. In this paper, the magnetic anisotropy of binder jet printed iron silicon samples is quantified and compared with commercial soft magnetic composite material.

[7] T. Q. Pham, C. Mellak, H. Suen, C. J. Boehlert, A. Muetze, P. Kwon, and S. N. Foster, "Binder jet printed iron silicon with low hysteresis loss," 2019 IEEE International Electric Machines & Drives Conference (IEMDC), 2019, pp. 1045-1052, doi: 10.1109/IEMDC.2019.8785256.

Abstract: In this paper, the iron loss characteristics of 3D printed iron silicon samples are compared with prototype soft magnetic composite material. Binder jet printing technology is used to prepare the iron silicon samples and its magnetic properties are experimentally extracted using the Epstein frame and the permeameter. It is shown that 3D printed samples can have lower hysteresis loss while achieving higher magnetic induction compared to prototype soft magnetic composites.

[8] T. Q. Pham, T. T. Do, P. Kwon and S. N. Foster, "Additive Manufacturing of High Performance Ferromagnetic Materials," 2018 IEEE Energy Conversion Congress and Exposition (ECCE), 2018, pp. 4303-4308, doi: 10.1109/ECCE.2018.8558245.

Abstract: Improving the efficiency, as well as reducing size of electrical machines, can reduce the amount and types of pollutants we emit into our environment; however, manufacturing realities often bottleneck the production of new low-cost and highly efficient motor designs. Additive manufacturing technologies provide flexibility to overcome limitations of the subtractive and powder metallurgical processes. In this paper, the magnetic characteristics of 3D printed iron silicon samples are compared with prototype soft magnetic composite material. Binder jet printing technology is used to prepare the iron silicon samples and its magnetic properties are experimentally extracted. It is shown that magnetic permeability of the 3D printed sample is higher than prototype soft magnetic composite.

4.3 Theses

[1] M. Meier, "Improving Cooling of an Axial Flux Permanent Magnet Machine Using Soft Magnetic Composites," PhD Thesis, Department of Electrical and Computer Engineering, Michigan State University, USA **Under preparation.**

[2] H. Suen, "Electrical Steels Fabricated by Binder Jet Printing," PhD Thesis, Department of Mechanical Engineering, Michigan State University, USA, **Under preparation.**

[3] T. Q. Pham, "A Feasibility Study of Non-Homogeneous Soft Magnetic Core for Electrical Machines - An Application of Additive Manufacturing," PhD Thesis, Department of Electrical and Computer Engineering, Michigan State University, USA, 2021. [Online]. Available: https://www.proquest.com/docview/2572591075

Abstract: The development of a new generation of energy efficient, high torque and power density electrical machines is part of a solution toward the global energy problem. An important step in improving electrical machine performance involves optimization of the machine geometry, winding configuration, and overcoming limitations within traditional magnetic materials. In electrical machine, the magnetic iron core accounts for a significant portion of its weight and size. Under a rotating magnetic field, conventional iron cores are subjected to a nonuniform magnetic field distribution. This leads to uneven saturation distribution, extra core loss, and sub-optimal utilization of the permeability at certain regions within the iron cores. Deploying materials with non-homogeneous magnetic permeability can lead to a more uniform magnetic flux density distribution and potentially better power density. Additionally, a multi-permeability iron core, where the permeability is tuned as a function of both position and electrical machine performance, can lead to a more efficient use of the core and an additional degree of freedom for core design. This work evaluates the use of iron cores with non-homogeneous magnetic permeability for electrical machines. It is numerically demonstrated that an iron core with spatially tuned permeability can be used to manipulate the airgap flux density waveform, torque, and iron loss in electrical machines.

Exploration and exploitation of non-homogeneous iron cores for electrical machines requires an accurate, low cost modelling technique. Finite element analysis can be used to model non-homogeneous iron cores but it can lead to an expensive computational requirement. Traditional magnetic equivalent circuits can provide quick estimation of the electrical machine performance in comparison to finite elements. However, this technique typically models just the main flux path and/or ignores the permeability in the iron cores. In this work, a technique is developed to model non-homogeneous, multi permeability iron cores in electrical machines. It is shown that the proposed technique closely approximates finite element results and reduces the simulation time nearly 80%. It is also demonstrated that the modelling technique can be integrated into a multi-objective optimization problem for development of novel iron cores.

Additive manufacturing, also known as 3D-printing, is a layer-based manufacturing technique which can fabricate unique, complex shapes. It also has the potential to fabricate non-homogeneous iron cores. Adoption of these complex iron cores for development of high performance electrical machines requires understanding of the magnetic properties and demonstration that printed iron cores can reach variable levels of permeability. In this work, the B-H characteristics are experimentally extracted using conventional magnetic characterization techniques. A simplified magnetic anisotropy test bed was developed to quantify levels of magnetic anisotropy. It is shown that 3D-printed iron cores can achieve different levels of relative permeability and low levels of magnetic anisotropy.

4.4 Invited Talks

[1] Shanelle N. Foster, "Electric Motors and Additive Manufacturing: An Inclusive Approach to Diversity Inspired Design," Town & Gown, East Lansing, Michigan, May 17, 2022, (Organizer: John Waller).

[2] Shanelle N. Foster, "3D Printed Electrical Steel: Opportunities and Challenges," University of Johannesburg, Department of Electrical Engineering Technology, Virtual, April 26, 2022, (Organizer: Mbika Muteba).

[3] Shanelle N. Foster, "3D Printed Magnetic Cores for Electrical Machines," IEEE Energy Conversion Congress & Expo, Virtual, October 14, 2021 (Organizers: Bulent Sarlioglu, Ayman El-Refaie, & Will Sixel).

Chapter 5

Training Opportunities

5.1 SEM Training for Electrical Engineers

Dr. Carl Boehlert, Professor of Chemical Engineering & Materials Science at MSU opened his scanning electron microscopy course to graduate and undergraduate students from the Department of Electrical & Computer Engineering working on this project. This course provided an introduction to microscopy and some of the equipment available at MSU. Beyond this course, a graduate student in the Department of Chemical Engineering & Materials Science continued to train electrical engineering graduate and undergraduate students to prepare samples for SEM. This training included polishing and mounting samples as well as use of ImageJ for optical density measurements. The MSU Composite Materials and Structure Center facilities manager/technician and materials science graduate students trained and electrical engineering graduate student to use additional microscopes.

5.2 Magnetic Characterization Training

As part of an independent study (2 credit course) Fall 2019, an undergraduate research assistant worked with a graduate student to setup the newly purchased Magnetic Instrumentation Soft Magnetic Tester, develop a guide for magnetic characterization of samples using the equipment and train other electrical engineering undergraduate research participants to perform magnetic characterization of 3D printed samples.

5.3 Genetic Algorithm and Finite Elements Training

A graduate student trained one of the undergraduate research participants to couple finite elements software to a python script to perform optimization using Non-Dominated Sorting Genetic Algorithm (NSGA). This student learned to model parts in finite elements as well as understand how genetic algorithms work.

Chapter 6

Participants

6.1 Faculty

i. **Shanelle N. Foster, PI**, Assistant Professor of Electrical and Computer Engineering, lead the project efforts. Dr. Foster supervised student participants from the Department of Electrical and Computer Engineering. She also provided guidance for magnetic and electrical characterization of the materials, sensitivity analysis, optimization, as well as on the design, numerical evaluation and assembly of electrical motors. She held weekly progress meetings with all student and faculty participants.

ii. **Patrick Kwon**, Professor of Mechanical Engineering and Director of the Laboratory for Advanced Manufacturing Processes at Michigan State University, provided guidance for fabrication of all samples using binder jet printing technology. Dr. Kwon supervised the student participant from the Department of Mechanical Engineering. He also participated in weekly project meetings.

iii. **Carl J. Boehlert**, Professor of Chemical Engineering and Materials Science, provided guidance for microstructural characterization. Dr. Boehlert supervised the student participants from the Department of Chemical Engineering and Materials Science. He also participated in weekly project meetings.

6.2 Graduate Students

i. **Thang Q. Pham** is a former PhD student in the MSU Department of Electrical and Computer Engineering. He was partially supported by this project. He earned his doctorate degree in 2021. His PhD thesis is titled "A Feasibility Study of Non-Homogeneous Soft Magnetic Core for Electrical Machines - An Application of Additive Manufacturing." Thang performed electrical and magnetic characterization of most of the 3D printed samples. He also assisted with preparing samples for microstructural characterization. He trained other students to perform magnetic and electrical characterization.

ii. **Hawke Suen** is a PhD student in the MSU Department of Mechanical Engineering. He prepared all of the 3D printed samples for characterization. He also completed density measurement by Archimedes method and tensile test. Additionally, he assisted with optical microscopy (OM), scanning electron microscopy (SEM) and energy dispersive spectroscopy (EDS). Hawke was partially supported by this project. He is working to complete his PhD thesis title "Electrical Steels Fabricated by Binder Jet Printing."

iii. **Geeta Kumari** is a PhD student in the MSU Department of Chemical Engineering and Materials Science. She performed microstructural characterization of the 3D printed samples. Optical microscopy (OM), scanning electron microscopy (SEM), energy dispersive spectroscopy (EDS), Transmission electron microscopy (TEM), x-ray diffraction (XRD) and Electron backscattered diffraction (EBSD) were the used for microstructural characterization of the 3D printed samples.

iv. **Tanzilur Rahman** is a PhD student in the MSU Department of Chemical Engineering and Materials Science. He assisted with microstructural characterization of the 3D printed samples. Scanning electron microscopy and Vickers microhardness measurements were used for microstructural characterization.

v. **Matt Meier** is a PhD student in the MSU Department of Electrical and Computer Engineering. He designed and assembled a permanent magnet motor with 3D printed magnetic core. The 3D printed magnetic core included embedded cooling channels. He experimentally evaluated performance of the permanent magnet motor. He is working to complete his PhD thesis titled "Improving Cooling of an Axial Flux Permanent Magnet Machine Using Soft Magnetic Composites" which includes comparison of the thermal performance of the 3D printed core to the soft magnetic composite (SMC) core.

vi. **Bhuvan Khoshoo** is a PhD student in the MSU Department of Electrical and Computer Engineering. He performed finite element simulations using the extracted properties of the 3D printed samples to evaluate performance of electrical machines. He also trained undergraduate students to use the Non-dominated Sorting Genetic Algorithm for optimization.

vii. **Khan Jazib Islam** is a MS student in the MSU Department of Electrical and Computer Engineering. He was partially supported by this project. He performed both magnetic and electrical characterization of 3D printed samples during the final year of the project.

viii. **Orwell Madovi** is a PhD student in the MSU Department of Electrical and Computer Engineering. He assisted with both magnetic and electrical characterization of 3D printed samples during the final year of the project.

6.3 Undergraduate Students

All of the undergraduate students were/are students in the Michigan State University, College of Engineering, Department of Electrical and Computer Engineering.

i. **Tia F. Smith** supported magnetic characterization of the 3D printed samples and SEM sample preparation. As part of an independent study course with the PI, Tia assisted with installation of the soft magnetic tester and prepared the guide used for training other students (both graduate and undergraduate) to use the equipment for extracting the magnetic properties of the 3D printed samples. Tia earned her B.S. degree in 2020.

ii. **Lauren Kaliszewski** assisted with magnetic characterization of the 3D printed samples and SEM sample preparation. Lauren earned her B.S. degree in 2020.

iii. **Josh Ward**, an ArcelorMittal Junior Fellow, assisted with magnetic characterization of the 3D printed samples. Josh earned his B.S. degree in 2020.

iv. **Jorge Peña** assisted with magnetic characterization of the 3D printed samples.

v. **Marcus Wolff**, an Honor's College Professorial Assistant, assisted with magnetic characterization of the 3D printed samples. He also assisted with design optimization using non-sorting genetic algorithm.

6.4 Other

Nicholas J. Jones is a Materials Engineer with the Naval Surface Warfare Center, Carderock Division. Dr. Jones helped us identify the carbon content in our 3D printed samples. He also reviewed some of our results and provided guidance.

Chapter 7

Honors and Awards

The PI, **Shanelle N. Foster**, was selected as a ***Mercator Fellow*** for a collaborative research center between TU Graz in Austria and TU Darmstadt in Germany to share her knowledge on the application of additive manufacturing to electrical machines. The research center, namely the Computational Electric Machine Laboratory, addresses the development of a model of the electrical machine required for accurate computation of the machine's electromagnetic, thermal and mechanical performance. This multidisciplinary, 4-year collaborative effort began June 2022.

The PI, **Shanelle N. Foster**, was awarded the ***2022 Emerging Accomplishments in Diversity Award*** by the Michigan State University College of Engineering March 2022 in recognition of her contributions to creating a diverse, equitable and inclusive environment within the department and college.

The PI, **Shanelle N. Foster**, was awarded a ***2021 NSF CAREER Award***. The project is titled "CAREER: An Inclusive Approach to Diversity Inspired Design on Novel 3D Printed Electric Motors" aims to close the knowledge gap for development of 3D printed motor components and leverage multi-material technologies to 3D print a complete working electric motor without compromising its performance or reliability. She was featured in May 2021 issue of *Electrical Apparatus: More than Motors* as well as on the local news, Fox47.

Joshua Ward, an undergraduate researcher, was selected as one of the ECE Department's Fall 2018 and Spring 2019 ***ArcelorMittal Junior Fellows***. This award provided him the opportunity to perform magnetic characterization of 3D printed samples.

Chapter 8

Technology Transfer

Nothing to report

Chapter 9

Future Plans

Eddy current loss in the developed 3D printed samples remains a challenge. Future work focuses on its reduction as well as increasing the magnetic saturation flux density. Development 3D printed rare-earth-free permanent magnets and topology optimization of electric machines are also included as future work.

Appendix A

Sample Preparation

Powder Composition	Fe	Si	$Fe_{91}Si_9$	FeSi alloy (6-10% Si)	B
Particle Size	90µm, avg. <10µm	1µm	44µm, mean 150µm, mean 14µm, mean 10µm, mean	15-45µm	1µm 500nm 100nm

Table A.1: Near spherical powders used for 3D printed samples

The linear packing model was used and compared to the measured packing density after tapping and mixing the powders [12]. Powders with the desired ratio were mixed in a high-speed mixer from Flacktek (Landrum, SC, USA) with 1500 RPM for 100 seconds.

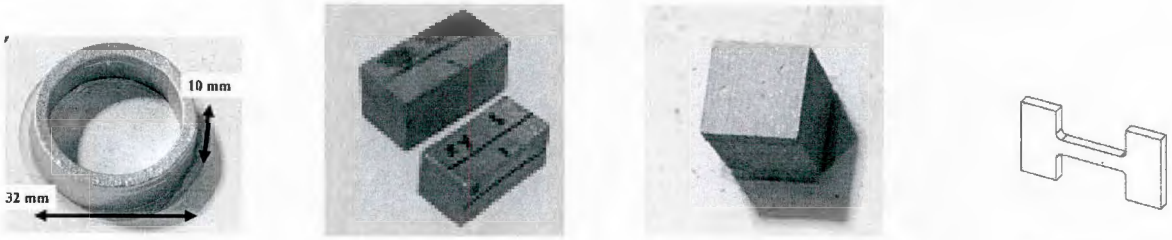

(a) Toroid (b) Cuboid (c) Cube (d) Dogbone

Figure A.1: Shapes of samples used for magnetic, electrical and microstructural characterization.

The X1-Lab from ExOne(North Huntington, PA, USA) was used to fabricate samples for magnetic, electrical and microstructural characterization. The shapes of samples used for each characterization are shown in Fig. A.1. Toroids and cubes are used for magnetic characterization. Cuboids are used for electrical characterization. Cubes and dogbones are used for microstructural characterization.

The printing process is illustrated in Fig. A.2. The printing parameter for the samples is set to a 2.3:1 feed powder ratio, and the layer thickness is set to 150µm. The saturation rate is 70%, assuming 60% of powder packing density. Furthermore, the initial rolling speed

is set to 0.3 mm/s. After printing, the green parts were placed in an air furnace at 195°C for 2 hours for curing. Then the samples were sintered in a carbon liner resistance furnace (Material research furnaces, Allenstown, NH) for 6 hours. Argon was used to evacuate the chamber and purge minimally three times. The heating and cooling rates are 5°C/min and 15°C/min, respectively.

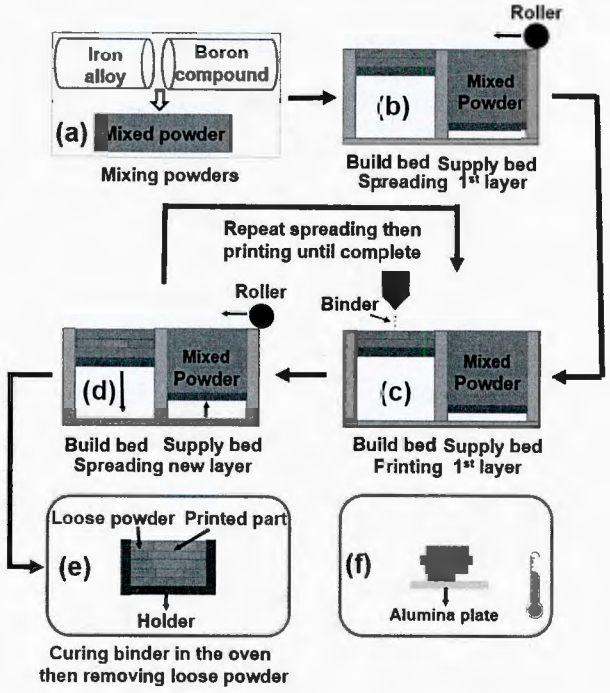

Figure A.2: Illustration of binder jet printing process

Appendix B

Characterization Techniques

Magnetic, electrical and microstructural characterization techniques used in this project are briefly described below.

B.1 Magnetic Characterization

The DC magnetic characterization is used to extract the initial magnetization curve and the hysteresis loop of the soft magnetic materials. The AC magnetic characterization extracts the frequency dependent $B-H$ curves and specific loss density curves.. The magnetic anisotropy characterization extracts the BH characteristics of the soft magnetic materials under different excitation directions. Magnetic characterization of these quantities provide insight on the performance of the materials of interest.

B.1.1 DC and AC Magnetic Characterization

Toroidal samples were wound with primary (outer layer) and secondary windings (inner layer). The DC and AC characteristics of each sample was extracted using a Magnetics Instrumentation Model SMT-700 Soft Magnetic Tester, [13,14]. The AC excitation frequency can be varied from the line frequency, 50 Hz up to 20000 Hz,. The excitation current is controlled such that the induced voltage remains within the sinusoidal waveform during the entire magnetization process. The quality of the sinusoidal signal is determined by the use of sinusoidal form factor value of $1.11 \pm 1\%$.

B.1.2 Magnetic Anisotropy Characterization

The main objective of the magnetic anisotropy characterization is to obtain the magnetization curves under excitation in the X-, Y-, and Z- directions. A simplified magnetic anisotropy characterization test bed, shown in Fig. B.1 was developed to provide magnetic anisotropy behaviors of the 3D printed samples [7].

B.2 Electrical Characterization

A four probe resistance measurement, shown in Fig. B.2 was used to assess the bulk resistivity.

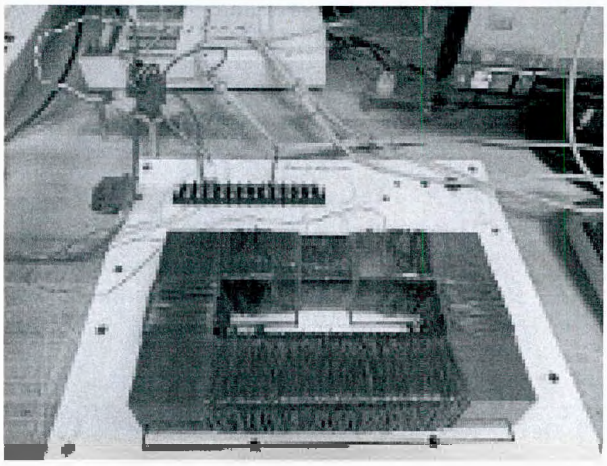

Figure B.1: Picture of experimental test bed used to characterize magnetic anistropy.

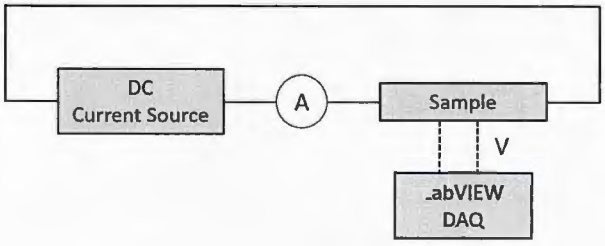

Figure B.2: Block diagram illustrating 4-point measurement: Kelvin bridge method.

B.3 Microstructural Characterization

The printed part's densities were calculated after sintering using Archimedes' principle in isopropyl alcohol (IPA).

All sintered samples were cut, mounted and metallographically prepared for microstructural evaluation. Samples were mechanically polished using through 400, 600, 800, 1200 US grit size (equivalent to FEPA 800, 1200, 2400, 4000 grit, respectively) SiC abrasive papers followed by diamond polishing with a polycrystalline diamond paste of 6, 3, 1, 1/4 µm particle size using IPA as the lubricant. The final polishing was performed using colloidal silica solution (0.025 µm crystallite size, 50% diluted with IPA).

Optical microscopy (OM), scanning electron microscopy (SEM), and x-ray diffraction (XRD) were used to characterize the microstructures. A Nikon eclipse MA200 optical microscope was used to take images for calculating the grain size using the line intercept method as per ASTM-E112-13. ImageJ software was used to help perform this calculation as well as the calculation of the volume fraction of the grain boundary phase present in the microstructures. XRD analysis was performed using a high-resolution Rigaku Ultima IV system equipped with a copper anode target (1.54Å). XRD patterns were collected with an accelerating voltage of 40 kV, beam intensity of 44 mA in a Bragg Brentano configuration, and a 0.008step size within the range of $20°<2\theta<120°$. The spectra collected were analyzed using Rigaku software. Using a Tescan Mira3 FEGSEM, both secondary electron (SE) and

backscattered electron (BSE) images were acquired. The typical SEM imaging conditions included a 20 keV beam voltage, a 17-mm working distance, and a 20-nm spot size. Energy dispersive spectroscopy (EDS) analysis was performed to investigate the composition of the phases inside the SEM using an acceleration voltage of 20 kV at a working distance of 12 mm. Electron backscattered diffraction (EBSD) orientation maps were collected using a Carl Zeiss Auriga SEM. These EBSD orientation maps were acquired at 20 keV beam voltage, working distances between 14 and 18 mm, and a step size of 2 µm with the specimen tilted 70° with respect to the electron beam. EBSD analysis software (EDAX TSL OIM analysis 6.1) was used to analyze the EBSD data considering 15°misorientations or higher as high-angle grain boundaries for grain size calculation. Vickers microhardness measurements were performed using Clark CM-800 AT on different regions of the samples with a load of 0.2 kgf and a dwell time of 15 s.

Differential scanning calorimetry (DSC) was conducted using Netzsch DSC model STA 449 F3 Nevio. A Platinum crucible with Al2O3 liner was used for heat-treatment. For inert environment, the reaction chamber was filled with argon with a continuous flow of 70mL/min. The temperature range and the heating rate used for data collection were 500-1300°C and 10K/min, respectively. The DSC helped in the identification of the phases and phase transformation as a function of the temperature.

REFERENCES

[1] T. Pham, P. Kwon, and S. Foster, "Additive manufacturing and topology optimization of magnetic materials for electrical machines—a review," *Energies*, vol. 14, no. 2, 2021. [Online]. Available: https://www.mdpi.com/1996-1073/14/2/283

[2] G. Kumari, T. Q. Pham, H. Suen, T. Rahman, P. Kwon, S. N. Foster, and C. J. Boehlert, "Improving the soft magnetic properties of binder jet printed iron-silicon alloy through boron addition," *Materials Chemistry and Physics*, under review.

[3] K. J. Islam, T. Q. Pham, H. Suen, G. Kumari, T. Rahman, C. J. Boehlert, P. Kwon, and S. N. Foster, "Eddy current loss reduction in binder jet printed iron silicon," in *2022 IEEE Energy Conversion Congress and Exposition (ECCE)*, accepted.

[4] B. Khoshoo, K. J. Islam, H. Suen, P. Kwon, J. Peña Lozano, and S. N. Foster, "Eddy current loss reduction in binder jet printed iron silicon cores," in *2022 International Conference on Electrical Machines (ICEM)*, accepted.

[5] T. Q. Pham, T. T. Do, P. Kwon, and S. N. Foster, "Additive manufacturing of high performance ferromagnetic materials," in *2018 IEEE Energy Conversion Congress and Exposition (ECCE)*, Sep. 2018, pp. 4303–4308.

[6] T. Q. Pham, C. Mellak, H. Suen, C. J. Boehlert, A. Muetze, P. Kwon, and S. N. Foster, "Binder jet printed iron silicon with low hysteresis loss," in *2019 IEEE International Electric Machines Drives Conference (IEMDC)*, May 2019, pp. 1045–1052.

[7] T. Q. Pham, H. Suen, P. Kwon, and S. N. Foster, "Characterization of magnetic anisotropy for binder jet printed Fe93.25Si6.75," in *2019 IEEE Energy Conversion Congress and Exposition (ECCE)*, Sep. 2019, pp. 745–752.

[8] T. Q. Pham, H. Suen, P. Kwon, and S. N. Foster, "Reduction in hysteresis loss of binder jet printed iron silicon," in *2020 International Conference on Electrical Machines (ICEM)*, vol. 1, 2020, pp. 1669–1675.

[9] T. Q. Pham and S. N. Foster, "Additive manufacturing of non-homogeneous magnetic cores for electrical machines opportunities and challenges," in *2020 International Conference on Electrical Machines (ICEM)*, vol. 1, 2020, pp. 1623–1629.

[10] T. Q. Pham and S. N. Foster, "Multi-permeability optimization approach for the iron core of a synchronous reluctance machine - an application of additive manufacturing," in *2021 IEEE Energy Conversion Congress and Exposition (ECCE)*, 2021, pp. 3852–3859.

[11] T. Q. Pham, H. Suen, P. Kwon, G. Kumari, C. J. Boehlert, and S. N. Foster, "Reduction in hysteresis loss of binder jet printed iron silicon with boron," *IEEE Transactions on Industry Applications*, vol. 57, no. 5, pp. 4864–4873, 2021.

[12] T. Stovall, F. de Larrard, and M. Buil, "Linear packing density model of grain mixtures," *Powder Technology*, vol. 48, no. 1, pp. 1–12, 1986. [Online]. Available: https://www.sciencedirect.com/science/article/pii/0032591086800584

[13] *Standard Test Method Alternating-Current Magnetic Properties of Toroidal Core Specimens Using the Voltmeter-Ammeter-Wattmeter Method*, ASTM International Std. ASTM A927/A927M-18, 2018.

[14] *Standard Test Method for Direct Current Magnetic Properties of Low Coercivity Magnetic Materials Using Hysteresigraphs*, ASTM International Std. ASTM A773/A773M-14, 2014.

REPORT DOCUMENTATION PAGE

1. REPORT DATE	2. REPORT TYPE	3. DATES COVERED	
		START DATE	END DATE
09-09-2022	Final	July 2018	September 2022

4. TITLE AND SUBTITLE

3D Printing of Magnetic Cores for Electrical Motors

5a. CONTRACT NUMBER	5b. GRANT NUMBER	5c. PROGRAM ELEMENT NUMBER
	N00014-18-1-2514	
5d. PROJECT NUMBER	**5e. TASK NUMBER**	**5f. WORK UNIT NUMBER**

6. AUTHOR(S)

Foster, Shanelle N.

7. PERFORMING ORGANIZATION NAME(S) AND ADDRESS(ES)

Michigan State University
426 Auditorium Road Rm 2
East Lansing, MI 48824-2600

8. PERFORMING ORGANIZATION REPORT NUMBER

N00014-18-1-2514-Final

9. SPONSORING/MONITORING AGENCY NAME(S) AND ADDRESS(ES)	10. SPONSOR/MONITOR'S ACRONYM(S)	11. SPONSOR/MONITOR'S REPORT NUMBER(S)
Office of Naval Research 875 N. Randolph Street Suite 1425 Arlington, VA 22203-1995	ONR	

12. DISTRIBUTION/AVAILABILITY STATEMENT

Approved for Public Release; Distribution is Unlimited.

13. SUPPLEMENTARY NOTES

Prepared in cooperation with Patrick Kwon, Carl J. Boehlert, Thang Q. Pham, Hawke Suen, Geeta Kumari, Tanzilur Rahman, Matt Meier, and Khan Jazib Islam.

14. ABSTRACT

This report briefly summarizes development of magnetic cores using binder jet printing technology via the investigation of the material magnetic properties. Eighty samples were prepared with different material compositions and process parameters. Soft magnetic composite material was used as the baseline comparison for this work primarily because SMC has been used for construction of unconventional motor topologies. The addition of boron as a sintering aid is shown to improve the performance of binder jet printed magnetic cores. Boron results in a eutectic reaction of Fe2B and Fe which shows as grain-boundary lamellae phase. The magnetic relative permeability of the optimized binder jet printed magnetic cores is nearly 6 times that of SMC. The optimized binder jet printed magnetic core also has lower hysteresis loss per cycle than commercially available SMC. The magnetic saturation flux density of the optimized binder jet printed magnetic core is 1.5T, similar to the maximum for commercially available SMC. A permanent magnet motor was designed and assembled using a binder jet printed magnetic core with cooling channels in each tooth. The motor was mounted and experimentally evaluated.

15. SUBJECT TERMS

3D printing; ferromagnetic core; magnetic characterization; binder jet printing; iron silicon alloy

16. SECURITY CLASSIFICATION OF:

a. REPORT	b. ABSTRACT	C. THIS PAGE	17. LIMITATION OF ABSTRACT	18. NUMBER OF PAGES
U	U	U	SAR	41

19a. NAME OF RESPONSIBLE PERSON	19b. PHONE NUMBER *(Include area code)*
Shanelle N. Foster	517-432-4589

INSTRUCTIONS FOR COMPLETING SF 298

1. REPORT DATE.
Full publication date, including day, month, if available. Must cite at least the year and be Year 2000 compliant, e.g. 30-06-1998; xx-06-1998; xx-xx-1998.

2. REPORT TYPE.
State the type of report, such as final, technical, interim, memorandum, master's thesis, progress, quarterly, research, special, group study, etc.

3. DATES COVERED.
Indicate the time during which the work was performed and the report was written.

4. TITLE.
Enter title and subtitle with volume number and part number, if applicable. On classified documents, enter the title classification in parentheses.

5a. CONTRACT NUMBER.
Enter all contract numbers as they appear in the report, e.g. F33615-86-C-5169.

5b. GRANT NUMBER.
Enter all grant numbers as they appear in the report, e.g. AFOSR-82-1234.

5c. PROGRAM ELEMENT NUMBER.
Enter all program element numbers as they appear in the report, e.g. 61101A.

5d. PROJECT NUMBER.
Enter all project numbers as they appear in the report, e.g. 1F665702D1257; ILIR.

5e. TASK NUMBER. Enter all task numbers as they appear in the report, e.g. 05; RF0330201; T4112.

5f. WORK UNIT NUMBER.
Enter all work unit numbers as they appear in the report, e.g. 001; AFAPL30480105.

6. AUTHOR(S). Enter name(s) of person(s) responsible for writing the report, performing the research, or credited with the content of the report. The form of entry is the last name, first name, middle initial, and additional qualifiers separated by commas, e.g. Smith, Richard, J, Jr.

7. PERFORMING ORGANIZATION NAME(S) AND ADDRESS(ES). Self-explanatory.

8. PERFORMING ORGANIZATION REPORT NUMBER.
Enter all unique alphanumeric report numbers assigned by the performing organization, e.g. BRL-1234; AFWL-TR-85-4017-Vol-21-PT-2.

9. SPONSORING/MONITORING AGENCY NAME(S) AND ADDRESS(ES). Enter the name and address of the organization(s) financially responsible for and monitoring the work.

10. SPONSOR/MONITOR'S ACRONYM(S). Enter, if available, e.g. BRL, ARDEC, NADC.

11. SPONSOR/MONITOR'S REPORT NUMBER(S). Enter report number as assigned by the sponsoring/monitoring agency, if available, e.g. BRL-TR-829; -215.

12. DISTRIBUTION/AVAILABILITY STATEMENT. Use agency-mandated availability statements to indicate the public availability or distribution limitations of the report. If additional limitations/ restrictions or special markings are indicated, follow agency authorization procedures, e.g. RD/ FRD, PROPIN, ITAR, etc. Include copyright information.

13. SUPPLEMENTARY NOTES. Enter information not included elsewhere such as: prepared in cooperation with; translation of; report supersedes; old edition number, etc.

14. ABSTRACT. A brief (approximately 200 words) factual summary of the most significant information.

15. SUBJECT TERMS. Key words or phrases identifying major concepts in the report.

16. SECURITY CLASSIFICATION. Enter security classification in accordance with security classification regulations, e.g. U, C, S, etc. If this form contains classified information, stamp classification level on the top and bottom of this page.

17. LIMITATION OF ABSTRACT. This block must be completed to assign a distribution limitation to the abstract. Enter UU (Unclassified Unlimited) or SAR (Same as Report). An entry in this block is necessary if the abstract is to be limited.